


Quasinormal Mode Spectroscopy via Horizon-Brightened Quantum Optics

Ali Övgün ^{1,*}

¹*Physics Department, Faculty of Arts and Sciences, Eastern Mediterranean University,
Famagusta, 99628 North Cyprus via Mersin 10, Türkiye.*

(Dated: November 12, 2025)

We develop a quantum optical framework for probing black hole quasinormal modes (QNMs) using two-level atoms in the spirit of the horizon-brightened acceleration radiation (HBAR) program. Starting from the QNM contribution to the Wightman function of a scalar field on a static, spherically symmetric black hole background, we derive the response function of a two-level Unruh–DeWitt detector following simple trajectories (static at fixed radius, with comments on radial free fall). The QNM sector imprints a set of Lorentzian resonances in the detector spectrum at the redshifted real parts of the QNM frequencies, with widths determined by the imaginary parts. We then treat a single dominant QNM as an effective non-Hermitian cavity mode coupled to an ensemble of driven two-level atoms, and derive a master equation of Dicke laser type. The resulting lasing threshold condition depends explicitly on the QNM damping rate, providing a direct quantum optical interpretation of the imaginary part of the QNM frequency. Specializing to the Schwarzschild geometry, we express the resonant frequencies, linewidths, and threshold in terms of photon-sphere data in the eikonal limit. We discuss several extensions and propose our framework as a unifying language connecting black hole ringdown, near-horizon conformal quantum mechanics, and quantum optics, thereby enriching the emerging program of black hole spectroscopy in the gravitational-wave era.

I. INTRODUCTION

Quantum field theory in curved spacetime predicts that horizons endow the vacuum with a highly nontrivial structure, giving rise to phenomena such as Unruh and Hawking radiation [1–3]. An especially sharp way to make this structure operational is through the response of localized particle detectors, typically modeled as Unruh–DeWitt (UDW) two-level systems coupled to quantum fields [4–6]. In this language, the notion of particles and temperature is encoded in detector transition probabilities and open-system dynamics rather than in global field modes, and the effects of acceleration, curvature, and horizons are directly reflected in the detector response.

Over the last decade, this operational viewpoint has merged with the toolbox of quantum optics and relativistic quantum information. Atoms, cavities, and interferometers are now widely used as theoretical probes of near-horizon physics and accelerated motion. A paradigmatic development is the “horizon-brightened acceleration radiation” (HBAR) program, in which clouds of two-level atoms falling into a Schwarzschild black hole in the Boulware vacuum are shown to emit a spectrum that is effectively thermal at the Hawking temperature, despite the global state not being thermal [7–15]. In this quantum-optical picture, the black hole acts as a kind of broadband quantum amplifier: infalling or accelerated atoms play the role of gain media, and their excitation and emission probabilities encode detailed information about the spacetime geometry and its thermodynamic properties. Closely related ideas have been sharpened in the near-horizon conformal quantum mechanics (CQM) framework, where the radial dynamics effectively reduces to an inverse-square potential in $0 + 1$ dimensions [16–18].

This emerging “relativistic quantum optics” program sits at the intersection of quantum information, quantum field theory, and gravitation. A broad class of works has analyzed accelerated or freely falling atoms, UDW detectors, and mirrors in flat and curved backgrounds, clarifying the relation between acceleration, detector response, and the equivalence principle [19–31]. These studies have been extended to Casimir setups and freely falling cavities or plates in gravitational fields [32–34], to light propagation in effective curved spaces and optical analogs [35–37], and to gravitational-wave and dynamical backgrounds where light–matter coupling is treated within Jaynes–Cummings–type models [38–41]. Collectively, these works demonstrate that relativistic motion and gravity imprint measurable signatures on atomic transition rates, interference fringes, and quantum correlations.

A central theme in this literature is the status of the equivalence principle and the gravitational mass of composite quantum systems. By comparing accelerated and freely falling detectors, mirror–atom configurations, and cavity setups, one can ask to what extent acceleration radiation and related phenomena are purely kinematic, or whether genuinely gravitational imprints survive [20–22, 42–46]. Near-horizon analyses have revealed universal instability and redshift mechanisms underlying quantum thermality [28, 47–49], while nonlocal and generalized field theories highlight

* ali.ovgun@emu.edu.tr

how the Unruh–Fulling effect is modified by ultraviolet completions [29, 31]. In parallel, density-operator methods have been developed to treat acceleration and vorticity within a unified thermodynamic formalism [30].

From a quantum-information perspective, acceleration and horizon physics have been explored through entanglement, steering, and Bell tests with relativistic detectors. Entanglement harvesting by pairs of accelerated or freely falling atoms, including along null trajectories and in black-hole backgrounds, reveals how curvature and horizon structure affect nonlocal correlations [45, 50–53]. Quantum steering ellipsoids and entropic measures characterize how Unruh noise reshapes quantum resources [54–56], while Bell-inequality violations in dynamical Casimir and circuit-QED platforms offer promising routes to simulate horizon-induced correlations in the laboratory [25, 26, 44, 57]. Proposals such as Ramsey interferometry witnesses of acceleration radiation [33, 58], shock-wave-induced quantum memories [59], and quantum amplifiers powered by black holes or horizons [12, 60–62] further deepen the analogy between gravitational horizons and nontrivial optical media.

Within this broader context, the HBAR program refines the UDW picture by focusing on atoms falling into, or hovering near, black-hole horizons and related causal boundaries. The emission and absorption spectra, together with the associated entropy production, encode a “horizon brightening” of acceleration radiation that depends on the near-horizon conformal structure and on the microscopic details of the coupling [7–11, 14, 18, 48, 63, 64]. This framework has now been applied to a wide variety of geometries, including quantum-corrected and braneworld black holes [14, 64–66], Kerr–Newman and rotating backgrounds [9, 39, 67], and scenarios where dark energy or dark matter fields modify the near-horizon region [40, 52, 68, 69]. Derivative couplings and their impact on acceleration radiation and HBAR entropy have been explored in detail [70, 71], and corrections arising from generalized uncertainty principles and renormalization-group improvements of the metric have been shown to leave characteristic imprints on HBAR entropy [64–66, 72].

Generalizations to Lorentz-violating and higher-curvature spacetimes open an additional window on fundamental physics. Acceleration radiation and HBAR-type quantities have been investigated for atoms in Lorentz-violating black-hole backgrounds, including Kalb–Ramond geometries, in order to identify potential observational signatures of symmetry breaking in the quantum regime [73–75]. Casimir-like probes and optical analogs in modified gravity provide complementary constraints on higher-derivative corrections and effective couplings [34–36]. At the same time, refined phase-space techniques and Wigner distributions in Rindler spacetime clarify the role of nonvacuum states and quantum coherence in acceleration phenomena [41, 76, 77]. Experimental and numerical advances, from water-wave analog horizons and accelerated-electron proposals for Unruh radiation to machine-learning-enhanced signal extraction in neutrino experiments, suggest that subtle acceleration-induced quantum effects may be within reach [37, 78, 79].

In parallel, the detection of gravitational waves from binary black-hole mergers by LIGO and Virgo has inaugurated the era of black-hole spectroscopy, in which the ringdown phase of the signal is analyzed to extract the quasinormal-mode (QNM) spectrum and test general relativity in the strong-field regime [80, 81]. QNMs encode the characteristic relaxation of a perturbed black hole through complex frequencies

$$\omega_{n\ell} = \Omega_{n\ell} - i\Gamma_{n\ell}, \quad (1)$$

whose real and imaginary parts determine, respectively, the oscillation frequencies and damping times [82, 83]. The prospect of *black-hole spectroscopy*—inferring the underlying geometry, mass, and spin from these spectral lines—has motivated extensive work on the structure and phenomenology of QNMs.

At the same time, there exists a mature and rapidly evolving body of research on the *classical* optical appearance of black holes, in particular their shadows and strong-field lensing properties. The shape and size of the black-hole shadow, as well as its deformation by spin, deviations from Kerr, higher-dimensional corrections, or braneworld effects, provide an independent probe of the geometry and of possible extensions of general relativity [84–93]. Studies of rotating non-Kerr spacetimes, plasmas around compact objects, and Gauss–Bonnet or braneworld black holes show how shadow and lensing observables respond to departures from the standard Kerr paradigm [90–93]. These imaging signatures complement the HBAR and acceleration-radiation program: while shadows and lensing probe the null-geodesic structure and effective refractive properties of the spacetime, quantum-optical probes via infalling atoms and cavities are sensitive to the detailed structure of quantum fields near the horizon. A consistent theoretical framework should ultimately relate these classical and quantum observables, providing a multi-channel spectroscopy of black holes.

These developments strongly suggest that QNMs, Hawking/Unruh physics, and quantum optics are deeply intertwined. On the one hand, QNMs appear as poles of the Green’s functions of perturbations in a black-hole background [94–96]. Quasinormal modes (QNMs) have been extensively studied as precise probes of black-hole spacetimes in a wide variety of backgrounds, including Schwarzschild–(A)dS, de Sitter, regular, and modified-gravity geometries, where scalar and gravitational perturbations reveal the impact of topology, nonlinearity, and higher-curvature terms on the spectrum [97–106]. The role of field content and rotation has been clarified through detailed analyses of massive scalar and vector fields, as well as eikonal-limit studies in Kerr and slowly rotating backgrounds, which connect

QNMs to superradiant instabilities and unstable null orbits [107–111]. On the methodological side, higher-order WKB schemes, continued-fraction techniques, and autocorrelation-based approaches provide efficient and accurate tools for computing spectra and greybody factors, and for assessing the physical significance of individual modes [97, 112–115]. More recently, loop-quantum-gravity-motivated corrections, regular black-hole models, and topological geometries have been used as test beds to investigate stability, spectral (in)stability, and potential echo signatures in the QNM spectrum [99, 116–119]. On the other hand, detector-based formulations of quantum field theory probe precisely those Green’s functions through response functions and open-system dynamics. Yet a systematic quantum-optical description in which QNMs play the role of effective cavity modes interacting with atomic degrees of freedom has not been fully developed.

In this work we propose and analyze such a framework, which we refer to as *HBAR-QNM spectroscopy*. The central idea is to regard the QNM contribution to the Wightman function as an effective discrete sector describing damped bosonic modes, and to couple this sector to a cloud of two-level atoms in the spirit of standard cavity quantum optics [120]. This enables us to import familiar concepts such as Lorentzian resonances, lasing thresholds, and Maxwell–Bloch equations into black-hole physics, and to reinterpret the imaginary parts of QNM frequencies as effective loss rates in a quantum-optical setting. More concretely, our main objectives are: To decompose the Wightman function into a QNM sector plus a continuum, where the QNM sector furnishes an effective discrete set of damped “cavity modes” with complex frequencies $\omega_n = \Omega_n - i\Gamma_n$, whose residues encode their spatial profiles [94–96]. To compute the response of two-level UDW detectors to this QNM sector. For static detectors, we show that QNMs produce Lorentzian resonances in the excitation rate at the locally redshifted QNM frequencies, with widths set by the redshifted damping rates. To treat a dominant QNM as a non-Hermitian bosonic mode coupled to an ensemble of pumped two-level atoms. A standard quantum-optical derivation then yields a Maxwell–Bloch system and a lasing threshold condition in which the imaginary part of the QNM plays the role of cavity loss. To specialize to the Schwarzschild geometry and express the spectroscopic signals in terms of photon-sphere quantities in the eikonal limit [121], thereby providing a geometric interpretation of the HBAR-QNM fingerprint.

Our treatment is deliberately idealized and should be viewed as a theoretical laboratory rather than an immediate observational proposal: we do not attempt to model realistic astrophysical environments or backreaction. Instead, our goal is to establish a coherent formal framework in which QNMs, detector response, and quantum-optical concepts can be discussed on equal footing. Within this framework, we can make explicit statements about how QNM damping rates enter lasing thresholds, how the near-horizon thermal behavior encoded in CQM combines with photon-sphere dynamics, and how different black-hole geometries lead to distinct HBAR-QNM spectral fingerprints.

The structure of the paper is as follows. In Sec. II we review the mode decomposition of a scalar field on a static, spherically symmetric black hole and isolate the QNM contribution to the positive-frequency Wightman function. In Sec. III we compute the response of a two-level UDW detector to this QNM sector and identify the resulting Lorentzian resonances. In Sec. IV we introduce an effective single-QNM master equation for a cloud of atoms coupled to a damped mode, derive the corresponding Maxwell–Bloch equations, and obtain a lasing threshold condition explicitly involving the QNM damping rate. In Sec. V we specialize to the Schwarzschild case, use photon-sphere data to approximate the QNM spectrum, and discuss the resulting HBAR-QNM spectral phenomenology. Section VI outlines illustrative figures and qualitative interpretations of our results, and we summarize and discuss extensions in Sec. VII.

Throughout, we work in units $c = G = k_B = \hbar = 1$, unless otherwise stated, and adopt the mostly-plus metric signature $(-, +, +, +)$.

II. QUASINORMAL-MODE CONTRIBUTION TO THE WIGHTMAN FUNCTION

In this section we briefly review the mode decomposition of a minimally coupled scalar field in a static, spherically symmetric black hole spacetime and recall how QNMs arise as poles of the Green’s function. Our goal is to isolate a QNM contribution to the positive-frequency Wightman function that will later serve as an effective discrete sector in the detector response.

We consider a static, spherically symmetric black hole background of the form

$$ds^2 = -f(r) dt^2 + f(r)^{-1} dr^2 + r^2 d\Omega^2, \quad (2)$$

where $d\Omega^2$ is the metric on the unit 2-sphere. The horizon is located at $r = r_h$, where $f(r_h) = 0$, and the corresponding surface gravity is

$$\kappa = \frac{1}{2} f'(r_h). \quad (3)$$

For concreteness we will later specialize to the Schwarzschild case, $f(r) = 1 - 2M/r$, but for now we keep $f(r)$ general.

We consider a real, minimally coupled scalar field Φ obeying the Klein–Gordon equation

$$\square\Phi = \frac{1}{\sqrt{-g}}\partial_\mu(\sqrt{-g}g^{\mu\nu}\partial_\nu\Phi) = 0, \quad (4)$$

and expand it in a complete set of normal modes adapted to the spherical symmetry and stationarity of the background.

We first decompose the field in spherical harmonics,

$$\Phi(t, r, \Omega) = \sum_{\ell=0}^{\infty} \sum_{m=-\ell}^{\ell} \frac{1}{r} \phi_{\ell m}(t, r) Y_{\ell m}(\Omega), \quad (5)$$

where Ω denotes the angular coordinates on the sphere and $Y_{\ell m}(\Omega)$ are the usual spherical harmonics. The prefactor $1/r$ is chosen so that the radial modes satisfy a Schrödinger-type equation.

Next we introduce the tortoise coordinate r_* , defined by

$$\frac{dr_*}{dr} = \frac{1}{f(r)}. \quad (6)$$

This maps the exterior region $r \in (r_h, \infty)$ to $r_* \in (-\infty, \infty)$, with the horizon at $r_* \rightarrow -\infty$ and spatial infinity at $r_* \rightarrow +\infty$. In terms of r_* , the radial dynamics takes a form reminiscent of scattering in one dimension.

Substituting Eq. (5) into the Klein–Gordon equation (4), we find that each partial wave $\phi_{\ell m}(t, r)$ satisfies a 1 + 1-dimensional wave equation,

$$\left(\frac{\partial^2}{\partial t^2} - \frac{\partial^2}{\partial r_*^2} + V_\ell(r) \right) \phi_{\ell m}(t, r) = 0, \quad (7)$$

where the effective potential for a minimally coupled scalar field is

$$V_\ell(r) = f(r) \left[\frac{\ell(\ell+1)}{r^2} + \frac{f'(r)}{r} \right]. \quad (8)$$

The first term is the centrifugal barrier, while the second encodes curvature effects. For other spins, the potential is modified in a known way [81, 122, 123], but the overall structure of Eq. (7) remains intact: each multipole propagates in an effective potential barrier that typically peaks near the photon sphere and decays towards the horizon and infinity.

It is often convenient to work in the frequency domain. Writing

$$\phi_{\ell m}(t, r) = \int_{-\infty}^{+\infty} \frac{d\omega}{2\pi} e^{-i\omega t} \psi_{\ell\omega}(r), \quad (9)$$

we obtain the ordinary differential equation

$$\left(-\frac{d^2}{dr_*^2} + V_\ell(r) \right) \psi_{\ell\omega}(r) = \omega^2 \psi_{\ell\omega}(r). \quad (10)$$

This equation defines a scattering problem in the potential $V_\ell(r)$, with incoming and outgoing components at the horizon and infinity.

The retarded Green's function for a fixed multipole ℓ can be represented in the time and frequency domains as

$$G_\ell^{\text{ret}}(t, r; r') = \int_{-\infty}^{+\infty} \frac{d\omega}{2\pi} e^{-i\omega t} g_\ell(\omega; r_*, r'_*), \quad (11)$$

where $g_\ell(\omega; r_*, r'_*)$ is built from two independent solutions of Eq. (10) satisfying appropriate boundary conditions (purely ingoing at the horizon and purely outgoing at infinity) and stitched together via the Wronskian [94, 95].

Quasinormal modes are defined as solutions of the homogeneous equation,

$$\left(-\frac{d^2}{dr_*^2} + V_\ell(r) \right) u_{n\ell}(r_*) = \omega_{n\ell}^2 u_{n\ell}(r_*), \quad (12)$$

subject to the boundary conditions of purely ingoing waves at the horizon and purely outgoing waves at spatial infinity. These conditions select a discrete set of complex frequencies

$$\omega_{n\ell} = \Omega_{n\ell} - i\Gamma_{n\ell}, \quad \Gamma_{n\ell} > 0, \quad (13)$$

reflecting the fact that perturbations decay over time due to radiation escaping to infinity or being absorbed by the horizon [80, 81].

Mathematically, QNMs correspond to poles of the Green's function in the complex frequency plane. One can deform the contour of integration in Eq. (11) into the lower half-plane, picking up contributions from these poles and from branch cuts associated with the continuous spectrum [94–96]. This yields a decomposition of the Green's function into a QNM sum plus a continuum (or “tail”) contribution. The same structure carries over to the positive-frequency Wightman function

$$G^+(x, x') = \langle 0 | \Phi(x) \Phi(x') | 0 \rangle, \quad (14)$$

where $|0\rangle$ denotes the chosen vacuum state (Boulware, Unruh, Hartle–Hawking, etc.).

Schematically, we may write

$$G^+(x, x') = G_{\text{QNM}}^+(x, x') + G_{\text{cont}}^+(x, x'), \quad (15)$$

where G_{QNM}^+ is a discrete sum over QNM poles and G_{cont}^+ is a continuum contribution sensitive to the choice of quantum state. The QNM part captures the dominant late-time ringdown behavior, while the continuum encodes power-law tails and thermal features.

A more explicit expression for the QNM contribution can be written as

$$G_{\text{QNM}}^+(x, x') \simeq \sum_{\ell m} \sum_n \mathcal{N}_{n\ell} \frac{u_{n\ell}(r_*) u_{n\ell}(r'_*)}{r r'} Y_{\ell m}(\Omega) Y_{\ell m}^*(\Omega') e^{-i\omega_{n\ell}(t-t')}, \quad (16)$$

where the coefficients $\mathcal{N}_{n\ell}$ are determined by the residues of the Green's function at the QNM poles and encode an appropriate normalization of the modes [94, 95, 124]. Equation (16) provides a QNM-based approximation to the two-point function that is valid in regimes where the discrete ringing dominates over the continuum.

For our purposes it is useful to focus on the correlation function evaluated at a fixed spatial point, which will later be taken as the location of a detector. We choose a fixed radius r_0 and angular position Ω_0 , and define the time difference

$$\Delta t := t - t'. \quad (17)$$

Evaluating Eq. (16) at $(r, \Omega) = (r_0, \Omega_0)$ and $(r', \Omega') = (r_0, \Omega_0)$, and summing over m , we can absorb the angular factors and mode residues into effective coefficients

$$B_n(r_0) := \sum_{\ell} \mathcal{N}_{n\ell} \frac{|u_{n\ell}(r_*^0)|^2}{r_0^2} \sum_{m=-\ell}^{\ell} |Y_{\ell m}(\Omega_0)|^2, \quad (18)$$

where $r_*^0 = r_*(r_0)$. We have reindexed the modes so that the label n runs over all relevant QNMs (including the multipole index ℓ , if desired). In terms of these coefficients, the QNM contribution to the Wightman function along a fixed spatial point reduces to

$$G_{\text{QNM}}^+(\Delta t; r_0) \equiv G_{\text{QNM}}^+(t, r_0, \Omega_0; t', r_0, \Omega_0) \simeq \sum_n B_n(r_0) e^{-i\omega_n \Delta t}, \quad (19)$$

where we denote the (relabelled) QNM frequencies by

$$\omega_n = \Omega_n - i\Gamma_n, \quad \Gamma_n > 0. \quad (20)$$

This simple exponential series will be the starting point for our analysis of detector response.

III. DETECTOR RESPONSE AND QNM RESONANCES

We now turn to the response of a two-level Unruh–DeWitt detector coupled to the field along a given trajectory $x(\tau)$, parameterized by the detector's proper time τ . Our goal is to show how the QNM sector of the Wightman function, Eq. (19), imprints Lorentzian resonances in the detector's excitation spectrum, localized at redshifted QNM frequencies and with linewidths determined by the damping rates.

A UDW detector is modeled as a two-level quantum system with ground and excited states $|g\rangle$ and $|e\rangle$, respectively, separated by an energy gap $\nu > 0$. In the interaction picture, the monopole operator of the detector can be written as

$$m(\tau) = \sigma_- e^{-i\nu\tau} + \sigma_+ e^{i\nu\tau}, \quad (21)$$

where $\sigma_+ = |e\rangle\langle g|$ and $\sigma_- = |g\rangle\langle e|$ are raising and lowering operators on the detector Hilbert space.

The detector couples to the scalar field along its worldline $x(\tau)$ via the interaction Hamiltonian

$$H_I(\tau) = g \chi(\tau) m(\tau) \Phi[x(\tau)], \quad (22)$$

where g is a small coupling constant and $\chi(\tau)$ is a real-valued switching function that controls the duration and smoothness of the interaction [6].

Assuming that the detector is initially in the ground state and the field in a vacuum state $|0\rangle$, the probability of excitation at leading order in perturbation theory is given by

$$P_{g \rightarrow e}(\nu) = g^2 \mathcal{F}(\nu), \quad (23)$$

where the *response function* is defined as [1–3]

$$\mathcal{F}(\nu) = \int_{-\infty}^{+\infty} d\tau \int_{-\infty}^{+\infty} d\tau' \chi(\tau) \chi(\tau') e^{-i\nu(\tau-\tau')} G^+(x(\tau), x(\tau')). \quad (24)$$

This expression explicitly shows how the detector response is determined by the two-point function of the field evaluated along the detector's trajectory. The exponential factor $e^{-i\nu(\tau-\tau')}$ implements energy conservation between the detector and the field, while the switching function ensures that the integral is finite and physically well-defined.

In stationary situations, where the Wightman function depends only on the proper-time difference $\tau - \tau'$ and the switching is slow, it is often convenient to define a transition rate,

$$\dot{\mathcal{F}}(\nu) = \lim_{T \rightarrow \infty} \frac{1}{T} \mathcal{F}(\nu), \quad (25)$$

which effectively reduces Eq. (24) to a one-dimensional Fourier transform in the difference variable.

We first consider a detector that is static at a fixed radius r_0 outside the black hole, with fixed angular position Ω_0 . Its worldline in Schwarzschild-like coordinates can be parameterized as

$$x^\mu(\tau) = (t(\tau), r_0, \Omega_0), \quad (26)$$

where the proper time τ and coordinate time t are related by gravitational redshift,

$$t(\tau) = \frac{\tau}{\sqrt{f(r_0)}}. \quad (27)$$

The static observer is accelerated with respect to free fall and therefore experiences a local temperature related to the Hawking temperature by a Tolman redshift factor [2, 3].

Along this trajectory, the coordinate-time difference between two events is

$$\Delta t = t(\tau) - t(\tau') = \frac{\Delta\tau}{\sqrt{f_0}}, \quad f_0 := f(r_0), \quad (28)$$

where $\Delta\tau = \tau - \tau'$. Restricting to the QNM sector (19), the Wightman function along the trajectory becomes

$$G_{\text{QNM}}^+(\tau, \tau') = \sum_n B_n(r_0) e^{-i\omega_n \Delta t} = \sum_n B_n(r_0) e^{-i\omega_n \Delta\tau / \sqrt{f_0}}. \quad (29)$$

For a long, adiabatic interaction (large effective measurement time), we may approximate the switching function as constant over a large interval and define the QNM contribution to the transition rate as

$$\dot{\mathcal{F}}_{\text{QNM}}(\nu) = \int_{-\infty}^{+\infty} d\Delta\tau e^{-i\nu\Delta\tau} G_{\text{QNM}}^+(\Delta\tau) = \sum_n B_n(r_0) \int_{-\infty}^{+\infty} d\Delta\tau e^{-i\nu\Delta\tau} e^{-i\omega_n \Delta\tau / \sqrt{f_0}}. \quad (30)$$

The integral over $\Delta\tau$ is a Fourier transform of a damped exponential. To make the damping explicit, we write

$$\omega_n = \Omega_n - i\Gamma_n, \quad \Gamma_n > 0, \quad (31)$$

so that

$$e^{-i\omega_n\Delta\tau/\sqrt{f_0}} = \exp\left[-i\frac{\Omega_n}{\sqrt{f_0}}\Delta\tau\right] \exp\left[-\frac{\Gamma_n}{\sqrt{f_0}}\Delta\tau\right]. \quad (32)$$

For $\Delta\tau > 0$, the second factor ensures convergence as long as $\Gamma_n > 0$, and a similar argument can be made for $\Delta\tau < 0$ using the standard $i\epsilon$ -prescription [2].

Focusing for the moment on the contribution from $\Delta\tau > 0$, we have

$$\int_0^\infty d\Delta\tau e^{-i\nu\Delta\tau} e^{-i\omega_n\Delta\tau/\sqrt{f_0}} = \int_0^\infty d\Delta\tau e^{-(\Gamma_n/\sqrt{f_0} + i[\nu + \Omega_n/\sqrt{f_0}])\Delta\tau} = \frac{1}{\Gamma_n/\sqrt{f_0} + i(\nu + \Omega_n/\sqrt{f_0})}. \quad (33)$$

Including the contribution from $\Delta\tau < 0$ and taking the real part yields a Lorentzian in frequency space. It is natural to define the *local* QNM frequency and damping rate as measured by the static observer at r_0 :

$$\omega_n^{(\text{loc})}(r_0) := \frac{\Omega_n}{\sqrt{f(r_0)}}, \quad \gamma_n^{(\text{loc})}(r_0) := \frac{\Gamma_n}{\sqrt{f(r_0)}}. \quad (34)$$

These are simply the global QNM parameters redshifted by the gravitational potential at the detector location.

Up to an overall normalization, we thus find that the contribution of mode n to the detector rate takes the Lorentzian form

$$\dot{\mathcal{F}}_n(\nu; r_0) \propto \frac{\gamma_n^{(\text{loc})}(r_0)}{(\nu - \omega_n^{(\text{loc})}(r_0))^2 + (\gamma_n^{(\text{loc})}(r_0))^2}. \quad (35)$$

Summing over all QNMs, we obtain the QNM-induced contribution to the detector response as

$$\dot{\mathcal{F}}_{\text{QNM}}(\nu; r_0) \simeq \sum_n \mathcal{A}_n(r_0) \frac{\gamma_n^{(\text{loc})}(r_0)}{(\nu - \omega_n^{(\text{loc})}(r_0))^2 + (\gamma_n^{(\text{loc})}(r_0))^2} \quad (36)$$

where the amplitudes $\mathcal{A}_n(r_0)$ are proportional to $|B_n(r_0)|^2$ and encode the overlap between the QNM spatial profile and the detector location. Equation (36) shows that, from the perspective of the static detector, the QNM sector manifests as a set of Lorentzian resonances at the locally redshifted real parts of the QNM frequencies, with linewidths given by the redshifted damping rates.

In a more complete description, the full detector spectrum includes both the QNM sector and the continuum/HBAR contribution. The latter provides an approximately thermal envelope determined by the local Hawking temperature

$$T_{\text{loc}}(r_0) = \frac{T_H}{\sqrt{f(r_0)}} = \frac{\kappa}{2\pi\sqrt{f(r_0)}}, \quad (37)$$

as emphasized in the HBAR and CQM analyses [7, 17, 63]. In this picture, the QNM resonances appear as sharp peaks superimposed on a broad thermal background, providing a spectrally resolved probe of the black hole's scattering properties.

We briefly comment on the case of a radially infalling detector, which is particularly relevant for the HBAR scenario. Consider, for example, an observer starting from rest at infinity in a Schwarzschild spacetime. The relation between coordinate time t and proper time τ along such a trajectory is more involved, but near the horizon it has the universal leading behavior

$$t(\tau) \sim -\frac{1}{\kappa} \ln(\tau_H - \tau) + \text{const}, \quad (38)$$

where τ_H is the finite proper time at which the detector crosses the horizon and κ is the surface gravity. Substituting this into the QNM phase factor yields

$$e^{-i\omega_n t(\tau)} \sim (\tau_H - \tau)^{i\omega_n/\kappa}, \quad (39)$$

so that the QNM contribution to the Wightman function along the trajectory acquires a characteristic power-law dependence on the proper time separation. This is precisely the type of structure that, in the HBAR analysis, leads to a thermal response with temperature T_H , arising from the logarithmic relation between proper time and the outgoing null coordinate [7, 63].

Incorporating the QNM phases into the contour integrals that appear in the rigorous evaluation of the response function (24) for infalling trajectories is technically more involved but conceptually straightforward. The net effect is expected to be a thermal spectrum with additional oscillatory features and modulations governed by the QNM parameters Ω_n and Γ_n . A full analytic treatment of this case, including the interplay between the QNM-induced resonances and the near-horizon CQM structure, is left for future work.

IV. SINGLE-QNM MASTER EQUATION AND LASING THRESHOLD

We now move beyond single-detector response and consider a many-body, quantum optical description in which a single dominant QNM is treated as an effective bosonic mode coupled to a cloud of driven two-level atoms. This setup is a natural generalization of the multimode master equations employed in the HBAR program [17, 63] and is closely related to the Dicke model of superradiance and lasing [120]. Our aim is to derive a Maxwell–Bloch system and a lasing threshold condition in which the QNM damping rate plays the role of cavity loss.

Motivated by the QNM expansion of the Green’s function, we model a single dominant QNM by an effective bosonic annihilation operator b with complex frequency

$$\omega_Q = \Omega_Q - i\Gamma_Q. \quad (40)$$

We work in a frame rotating at frequency Ω_Q , so that the free Hamiltonian for the QNM mode can be written as

$$H_{\text{field}} = \hbar\Delta_c b^\dagger b, \quad (41)$$

where $\Delta_c := \omega_{\text{lab}} - \Omega_Q$ denotes a small detuning with respect to some laboratory or driving frequency (we will set $\Delta_c \approx 0$ near resonance). The imaginary part $-\Gamma_Q$ corresponds to an effective decay rate, which we incorporate at the level of the master equation through a Lindblad term

$$\mathcal{L}_{\text{QNM}}[\rho] = \kappa \left(2b\rho b^\dagger - b^\dagger b\rho - \rho b^\dagger b \right), \quad \kappa \sim 2\Gamma_Q + \kappa_{\text{extra}}, \quad (42)$$

where ρ is the density matrix of the combined system and κ_{extra} accounts for additional environmental losses (e.g. coupling to other field modes or absorption by external media).

We consider N identical two-level atoms with transition frequency ν , described by Pauli operators σ_j^\pm, σ_j^z ($j = 1, \dots, N$) and Hamiltonian

$$H_{\text{atoms}} = \frac{\hbar\nu}{2} \sum_{j=1}^N \sigma_j^z. \quad (43)$$

The atom–QNM interaction is modeled by a Dicke-type Hamiltonian

$$H_{\text{int}} = \hbar g \sum_{j=1}^N (\sigma_j^+ b + \sigma_j^- b^\dagger), \quad (44)$$

where g is an effective coupling constant that includes overlap factors between the QNM spatial profile and the atomic cloud, as well as local gravitational redshift factors.

The atoms are taken to interact with additional reservoirs that provide pumping and relaxation processes. At the level of the master equation, these are described phenomenologically by

$$\mathcal{L}_{\text{atoms}}[\rho] = \sum_{j=1}^N (\gamma_\downarrow D[\sigma_j^-]\rho + \gamma_\uparrow D[\sigma_j^+]\rho), \quad (45)$$

where

$$D[L]\rho = L\rho L^\dagger - \frac{1}{2}\{L^\dagger L, \rho\} \quad (46)$$

is the standard Lindblad dissipator, and $\gamma_\uparrow, \gamma_\downarrow$ are excitation and relaxation rates, respectively. A nonzero population inversion corresponds to $\gamma_\uparrow > \gamma_\downarrow$ and is essential for lasing.

Collecting all contributions, the full master equation for the reduced density matrix of the QNM mode plus atomic cloud reads

$$\dot{\rho} = -\frac{i}{\hbar}[H_{\text{field}} + H_{\text{atoms}} + H_{\text{int}}, \rho] + \mathcal{L}_{\text{QNM}}[\rho] + \mathcal{L}_{\text{atoms}}[\rho]. \quad (47)$$

This is a standard open quantum system description, now with the key novelty that the cavity mode is identified with a damped QNM of the black hole background.

To derive a lasing threshold condition, we adopt a semiclassical treatment in which we replace operator expectation values by c-numbers and factorize higher-order correlations. We introduce the collective variables

$$\alpha := \langle b \rangle, \quad P := \sum_{j=1}^N \langle \sigma_j^- \rangle, \quad D := \sum_{j=1}^N \langle \sigma_j^z \rangle, \quad (48)$$

which play the roles of field amplitude, collective polarization, and total inversion, respectively. Under the usual mean-field approximations (e.g. $\langle b\sigma_j^z \rangle \approx \langle b \rangle \langle \sigma_j^z \rangle$), the equations of motion derived from Eq. (47) reduce to the familiar Maxwell–Bloch equations [120]:

$$\dot{\alpha} = -(\kappa + i\Delta_c)\alpha + gP, \quad (49)$$

$$\dot{P} = -(\gamma_\perp + i\Delta_a)P + gD\alpha, \quad (50)$$

$$\dot{D} = -\gamma_\parallel(D - ND_0) - 2g(\alpha^*P + \alpha P^*), \quad (51)$$

where

$$\Delta_a := \nu - \Omega_Q \quad (52)$$

is the atom–QNM detuning, and $\gamma_\perp, \gamma_\parallel$ are transverse and longitudinal relaxation rates, respectively, given in terms of $\gamma_\uparrow, \gamma_\downarrow$ and any additional dephasing processes. The equilibrium inversion per atom in the absence of the field is

$$D_0 := \frac{\gamma_\uparrow - \gamma_\downarrow}{\gamma_\uparrow + \gamma_\downarrow}, \quad (53)$$

so that in the absence of coupling to the field we have $D = ND_0$.

Equations (49)–(51) describe the coupled dynamics of the QNM mode and the atomic ensemble. The interplay between gain (controlled by g^2ND_0) and loss (controlled by κ and γ_\perp) determines whether a coherent macroscopic occupation of the QNM mode can develop.

The “off” (non-lasing) state of the system corresponds to

$$\alpha = 0, \quad P = 0, \quad D = ND_0, \quad (54)$$

i.e. no coherent field, no polarization, and a uniform inversion. To determine whether this state is stable or unstable to small perturbations, we linearize Eqs. (49)–(51) around it, neglecting the nonlinear saturation term in Eq. (51). We obtain

$$\dot{\alpha} = -(\kappa + i\Delta_c)\alpha + gP, \quad (55)$$

$$\dot{P} = -(\gamma_\perp + i\Delta_a)P + gND_0\alpha. \quad (56)$$

Looking for solutions of the form $\alpha, P \propto e^{\lambda t}$, we find the eigenvalue equation

$$\begin{pmatrix} \lambda + \kappa + i\Delta_c & -g \\ -gND_0 & \lambda + \gamma_\perp + i\Delta_a \end{pmatrix} \begin{pmatrix} \alpha \\ P \end{pmatrix} = 0, \quad (57)$$

which leads to the characteristic polynomial

$$(\lambda + \kappa + i\Delta_c)(\lambda + \gamma_\perp + i\Delta_a) - g^2ND_0 = 0. \quad (58)$$

To obtain a simple threshold condition, we consider the near-resonant case

$$\Delta_c \approx 0, \quad \Delta_a \approx 0, \quad (59)$$

so that the QNM mode and atomic transition are approximately frequency-matched. Then Eq. (58) reduces to

$$(\lambda + \kappa)(\lambda + \gamma_\perp) - g^2 N D_0 = 0. \quad (60)$$

The boundary between stability and instability is reached when the real part of the leading eigenvalue λ crosses zero. Setting $\lambda = 0$ yields the lasing threshold condition

$$\boxed{g^2 N D_0^{(\text{thr})} = \kappa \gamma_\perp} \quad (61)$$

or, equivalently,

$$D_0^{(\text{thr})} = \frac{\kappa \gamma_\perp}{g^2 N}. \quad (62)$$

Equation (61) is the central result of this section: it directly relates the minimal inversion per atom required for lasing to the cavity loss rate κ and the atomic coherence decay rate γ_\perp .

In our black hole context, the effective cavity loss rate is dominated by the QNM damping,

$$\kappa \sim 2\Gamma_Q + \kappa_{\text{extra}}, \quad (63)$$

where the factor of 2 reflects the relation between the QNM imaginary part and the energy decay rate, and κ_{extra} subsumes additional loss channels. Thus the *imaginary part* of the QNM frequency plays precisely the role of a cavity loss rate that must be compensated by gain from the inverted atomic ensemble. Equation (61) therefore furnishes a direct quantum optical interpretation of the QNM damping rate: more strongly damped modes require a larger inversion to reach threshold and lase.

Above threshold, the nonlinear saturation term in Eq. (51) stabilizes the field amplitude at a finite value, corresponding to a coherent QNM-dominated state. The stationary solutions and their stability properties can be analyzed by solving the steady-state Maxwell–Bloch equations and studying small perturbations around them [120]. While such an analysis is straightforward, it is beyond the scope of the present work, where our primary focus is on the threshold condition itself and its dependence on QNM properties.

V. SCHWARZSCHILD CASE AND HBAR–QNM SPECTROSCOPY

We now specialize our framework to the Schwarzschild geometry, where the QNM spectrum is particularly well understood and admits a simple approximation in the eikonal (large- ℓ) limit. This allows us to make our discussion more concrete and to relate the HBAR–QNM features directly to photon-sphere quantities.

For a Schwarzschild black hole of mass M , the metric function is

$$f(r) = 1 - \frac{2M}{r}. \quad (64)$$

The unstable photon sphere is located at the radius

$$r_c = 3M, \quad (65)$$

where null circular geodesics exist. In the eikonal (large- ℓ) limit, the QNM frequencies for various spins are governed by properties of this photon sphere [121]. Specifically, one finds

$$\Omega_{n\ell} \approx \ell \Omega_c, \quad \Gamma_{n\ell} \approx (n + \tfrac{1}{2}) \lambda_c, \quad (66)$$

where

$$\Omega_c = \sqrt{\frac{f(r_c)}{r_c^2}} = \frac{1}{3\sqrt{3}M}, \quad (67)$$

is the orbital frequency of the null circular orbit, and

$$\lambda_c = \sqrt{\frac{f(r_c)}{2r_c^2} (2f(r_c) - r_c^2 f''(r_c))} = \frac{1}{3\sqrt{3}M} \quad (68)$$

is the corresponding Lyapunov exponent controlling the instability of the orbit. Thus, to leading order in the eikonal expansion, the QNM spectrum takes the simple form

$$\omega_{n\ell} \approx \frac{\ell - i(n + \frac{1}{2})}{3\sqrt{3}M}. \quad (69)$$

This relation, together with Eq. (34), provides a direct link between the Schwarzschild QNM parameters and the HBAR–QNM spectroscopic features measured by a detector at radius r_0 .

For a static detector at $r_0 > 2M$, the locally measured QNM frequencies and damping rates are

$$\omega_{n\ell}^{(\text{loc})}(r_0) = \frac{\Omega_{n\ell}}{\sqrt{1 - 2M/r_0}}, \quad \gamma_{n\ell}^{(\text{loc})}(r_0) = \frac{\Gamma_{n\ell}}{\sqrt{1 - 2M/r_0}}. \quad (70)$$

Substituting into Eq. (36), we see that the detector response exhibits Lorentzian resonances at

$$\nu \approx \omega_{n\ell}^{(\text{loc})}(r_0), \quad (71)$$

with linewidths set by $\gamma_{n\ell}^{(\text{loc})}(r_0)$. As the detector moves closer to the photon sphere, the amplitudes $\mathcal{A}_n(r_0)$ are expected to increase, reflecting the stronger overlap with the QNM spatial profiles.

A. HBAR envelope and QNM resonances

Within the HBAR framework, the detector also experiences a broad thermal-like response governed by the local Hawking temperature. For Schwarzschild, the Hawking temperature is

$$T_H = \frac{1}{8\pi M}, \quad (72)$$

and the local Tolman-redshifted temperature at radius r_0 is

$$T_{\text{loc}}(r_0) = \frac{T_H}{\sqrt{1 - 2M/r_0}}. \quad (73)$$

The continuum contribution $\dot{\mathcal{F}}_{\text{therm}}(\nu; T_{\text{loc}})$ arising from near-horizon CQM and the Boulware vacuum structure yields a smooth, approximately Planckian envelope in the detector spectrum [7, 16, 17, 63]. The precise functional form depends on the trajectory and switching, but its qualitative features are those of a thermal distribution at temperature T_{loc} .

Combining the thermal envelope with the QNM-induced resonances, we obtain a schematic form for the total detector response:

$$\dot{\mathcal{F}}(\nu; r_0) \approx \dot{\mathcal{F}}_{\text{therm}}(\nu; T_{\text{loc}}) + \dot{\mathcal{F}}_{\text{QNM}}(\nu; r_0), \quad (74)$$

where $\dot{\mathcal{F}}_{\text{QNM}}$ is given by Eq. (36). We refer to this combination—thermal envelope decorated by discrete QNM Lorentzians—as the *HBAR–QNM spectroscopic fingerprint* of the black hole.

In the single-mode lasing picture developed in Sec. IV, the Schwarzschild QNM damping rate Γ_Q enters the threshold condition (61) via

$$\kappa \sim 2\Gamma_Q + \kappa_{\text{extra}}, \quad (75)$$

so that the minimal inversion required to stimulate a macroscopic occupation of the QNM mode is directly sensitive to photon-sphere properties. Different black hole spacetimes (e.g. regular black holes, non-linear electrodynamics solutions, or modified-gravity backgrounds) generally have different photon-sphere radii, orbital frequencies, and Lyapunov exponents [121], and hence different QNM spectra and lasing thresholds. In this way, the combined HBAR–QNM fingerprint offers a robust method of distinguishing between Schwarzschild and other Schwarzschild-like metrics at the level of their microscopic quantum optical signatures.

The distinct physical origins and properties of the thermal and QNM components of the detector signal are summarized in Table I.

TABLE I. Comparison of the HBAR continuum and QNM resonance components of the detector signal. These two components are sourced by distinct physics at different locations: the continuum by near-horizon CQM, and the discrete resonances by photon-sphere dynamics.

Feature	HBAR Continuum Component	QNM Resonance Component
Signal Type	Thermal continuum	Discrete resonances
Spectral Shape	Broad (Planckian-like)	Narrow (Lorentzian)
Correlator Origin	$G_{\text{cont}}^+(x, x')$ (branch cut)	$G_{\text{QNM}}^+(x, x')$ (poles)
Geometric Origin	Near-horizon region ($r \approx r_h$)	Photon sphere ($r \approx r_c$)
Governing Physics	Conformal quantum mechanics (CQM)	Null geodesic instability
Primary Parameters	Hawking temperature $T_H = \kappa/(2\pi)$	QNM frequencies $\{\Omega_n, \Gamma_n\}$

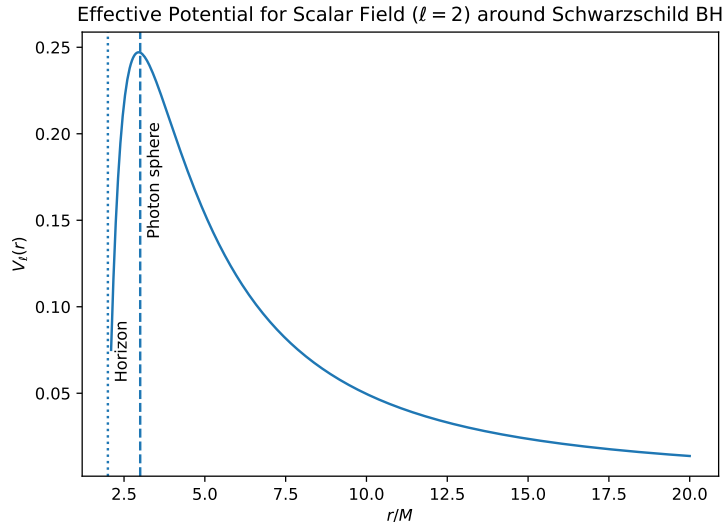


FIG. 1. Schematic representation of the setup. A static or infalling cloud of two-level atoms interacts with the scalar field on a black hole background. The effective potential $V_\ell(r)$ forms a barrier around the photon sphere, supporting quasinormal modes with complex frequencies $\omega_{n\ell}$. The atoms experience a thermal HBAR background due to near-horizon physics, as well as discrete QNM-induced resonances.

VI. FIGURES AND QUALITATIVE DISCUSSION

In this section we briefly describe a set of illustrative figures that help visualize the HBAR–QNM framework and its physical implications. These figures can be generated analytically in the eikonal approximation or numerically using standard QNM codes [80, 94].

A. Schematic geometry and QNM–HBAR setup

Figure 1 shows a black hole with its effective potential barrier around the photon sphere, along with a cloud of two-level atoms. The potential barrier supports quasinormal ringing as waves are transiently trapped and leak out to infinity or into the horizon. At the same time, atoms in the near-horizon region probe the conformal structure responsible for HBAR thermality. This geometric picture highlights the two-scale nature of the problem: the horizon sets the temperature and thermal envelope, while the photon sphere fixes the QNM frequencies and damping that appear as discrete spectral features.

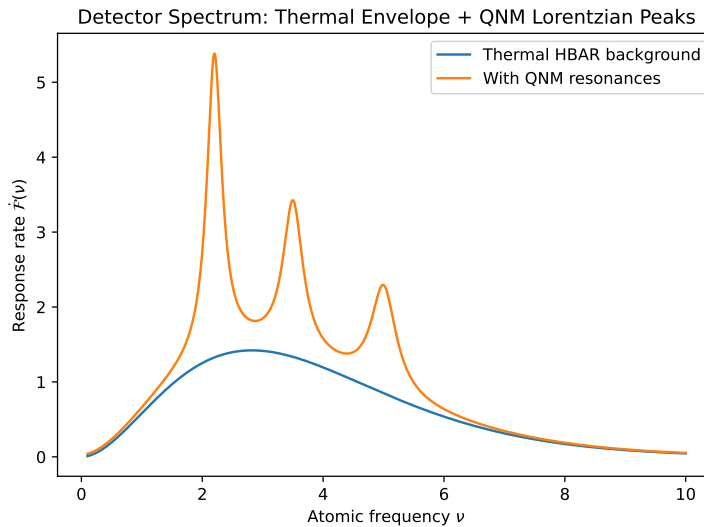


FIG. 2. Detector response rate $\dot{\mathcal{F}}(\nu)$ as a function of atomic frequency ν for a static detector at fixed radius r_0 outside a Schwarzschild black hole. The smooth curve corresponds to the thermal HBAR background at local temperature T_{loc} ; the superimposed peaks are Lorentzian resonances at the locally redshifted QNM frequencies $\omega_{n\ell}^{(\text{loc})}(r_0)$. The widths of the peaks encode the QNM damping rates.

B. Detector spectrum and QNM resonances

Figure 2 shows a representative detector spectrum. The broad background is approximately Planckian, with its slope determined by T_{loc} . Superimposed on this envelope are several narrow peaks at discrete frequencies corresponding to $\omega_{n\ell}^{(\text{loc})}(r_0)$. As the detector moves closer to the horizon, both the thermal envelope and the resonances are redshifted and broadened in a correlated way. Measuring the positions and widths of these peaks as a function of radius provides direct access to $\Omega_{n\ell}(M)$ and $\Gamma_{n\ell}(M)$, and hence to the underlying photon-sphere parameters Ω_c and λ_c .

VII. CONCLUSIONS AND OUTLOOK

We have proposed and developed a quantum optical framework in which black hole quasinormal modes are probed and manipulated by two-level atoms in the spirit of the HBAR program. Our main results can be summarized as follows: Starting from a QNM expansion of the Wightman function, we derived the QNM contribution to the response of a two-level Unruh–DeWitt detector. For a static detector, the QNM sector yields a series of Lorentzian resonances at the locally redshifted real parts of the QNM frequencies, with widths determined by the redshifted imaginary parts. Treating a single dominant QNM as an effective bosonic mode coupled to an ensemble of pumped two-level atoms, we obtained a Maxwell–Bloch system and derived a lasing threshold condition $g^2 N D_0^{(\text{thr})} = \kappa \gamma_{\perp}$, where the effective cavity loss rate $\kappa \sim 2\Gamma_Q + \kappa_{\text{extra}}$ is directly related to the imaginary part of the QNM frequency. This provides a quantum optical interpretation of QNM damping. Specializing to Schwarzschild, we expressed the leading QNM frequencies and damping rates in terms of photon-sphere quantities and described the resulting HBAR–QNM spectrum: a thermal envelope with superimposed QNM resonances. We argued that this “HBAR–QNM fingerprint” can distinguish Schwarzschild from other Schwarzschild-like metrics and encodes both near-horizon CQM and photon-sphere dynamics.

Our analysis opens several avenues for further works. Extending the master equation to multiple QNMs and to entangled atomic ensembles would open an avenue to studying entanglement transfer and decoherence in QNM-dominated regimes, and to exploring connections with non-Hermitian and parity-time symmetric quantum optics, as well as with black-hole laser scenarios in analogue gravity systems. Analogue gravity platforms (e.g. optical, acoustic, or Bose–Einstein condensate analogues) and engineered optical cavities with tailored loss profiles might realize aspects of the QNM–lasing scenario explored here, providing experimental access to related phenomena in a controlled setting. Although our framework is theoretical and idealized, the formal parallels between HBAR–QNM spectroscopy and gravitational-wave ringdown suggest that techniques developed here may inspire new ways of interpreting ringdown

data, especially in the context of multi-mode reconstruction and tests of the no-hair theorem.

We view the present work as a first step toward a systematic quantum optical theory of black hole ringdown and spectroscopy, in which QNMs are not only passive signatures of spacetime curvature but active participants in a rich non-equilibrium quantum dynamics. Further development along these lines may shed new light on the interplay between gravity, thermodynamics, and quantum information in the strong-field regime.

ACKNOWLEDGMENTS

A. Ö. would like to acknowledge networking support of the COST Action CA21106 - COSMIC WISPerS in the Dark Universe: Theory, astrophysics and experiments (CosmicWISPerS), the COST Action CA22113 - Fundamental challenges in theoretical physics (THEORY-CHALLENGES), the COST Action CA21136 - Addressing observational tensions in cosmology with systematics and fundamental physics (CosmoVerse), the COST Action CA23130 - Bridging high and low energies in search of quantum gravity (BridgeQG), and the COST Action CA23115 - Relativistic Quantum Information (RQI) funded by COST (European Cooperation in Science and Technology). A. Ö. also thanks to EMU, TUBITAK, ULAKBIM (Turkiye) and SCOAP3 (Switzerland) for their support.

-
- [1] W. G. Unruh, “Notes on black hole evaporation,” *Phys. Rev. D* **14**, 870 (1976).
 - [2] N. D. Birrell and P. C. W. Davies, *Quantum Fields in Curved Space*, Cambridge Monographs on Mathematical Physics (Cambridge University Press, Cambridge, UK, 1982).
 - [3] Luis C. B. Crispino, Atsushi Higuchi, and George E. A. Matsas, “The Unruh effect and its applications,” *Rev. Mod. Phys.* **80**, 787–838 (2008), [arXiv:0710.5373 \[gr-qc\]](#).
 - [4] B.S. DeWitt, *Quantum gravity: the new synthesis* (University Press., 1979) pp. p. 680–745.
 - [5] Shin Takagi, “Vacuum Noise and Stress Induced by Uniform Acceleration: Hawking-Unruh Effect in Rindler Manifold of Arbitrary Dimension,” *Prog. Theor. Phys. Suppl.* **88**, 1–142 (1986).
 - [6] Jorma Louko and Alejandro Satz, “How often does the Unruh-DeWitt detector click? Regularisation by a spatial profile,” *Class. Quant. Grav.* **23**, 6321–6344 (2006), [arXiv:gr-qc/0606067](#).
 - [7] Marlan O. Scully, Stephen Fulling, David Lee, Don N. Page, Wolfgang Schleich, and Anatoly Svidzinsky, “Quantum optics approach to radiation from atoms falling into a black hole,” *Proc. Nat. Acad. Sci.* **115**, 8131–8136 (2018), [arXiv:1709.00481 \[quant-ph\]](#).
 - [8] H. E. Camblong, A. Chakraborty, and C. R. Ordóñez, “Near-horizon aspects of acceleration radiation by free fall of an atom into a black hole,” *Phys. Rev. D* **102**, 085010 (2020), [arXiv:2009.06580 \[gr-qc\]](#).
 - [9] A. Azizi, H. E. Camblong, A. Chakraborty, C. R. Ordóñez, and M. O. Scully, “Acceleration radiation of an atom freely falling into a Kerr black hole and near-horizon conformal quantum mechanics,” *Phys. Rev. D* **104**, 065006 (2021), [arXiv:2011.08368 \[gr-qc\]](#).
 - [10] A. Azizi, H. E. Camblong, A. Chakraborty, C. R. Ordóñez, and M. O. Scully, “Quantum optics meets black hole thermodynamics via conformal quantum mechanics: I. Master equation for acceleration radiation,” *Phys. Rev. D* **104** (2021), [10.1103/PhysRevD.104.084086](#), [arXiv:2108.07570 \[gr-qc\]](#).
 - [11] A. Azizi, H. E. Camblong, A. Chakraborty, C. R. Ordóñez, and M. O. Scully, “Quantum optics meets black hole thermodynamics via conformal quantum mechanics: II. Thermodynamics of acceleration radiation,” *Phys. Rev. D* **104** (2021), [10.1103/PhysRevD.104.084085](#), [arXiv:2108.07572 \[gr-qc\]](#).
 - [12] Marlan O. Scully, Anatoly Svidzinsky, and William Unruh, “On Bose–Einstein Condensation and Unruh–Hawking Radiation from a Quantum Optical Perspective,” *J. Low Temp. Phys.* **208**, 160–171 (2022).
 - [13] Marlan O. Scully, Anatoly Svidzinsky, and William Unruh, “Entanglement in Unruh, Hawking, and Cherenkov radiation from a quantum optical perspective,” *Phys. Rev. Res.* **4**, 033010 (2022).
 - [14] Ashmita Das, Soham Sen, and Sunandan Gangopadhyay, “Horizon brightened accelerated radiation in the background of braneworld black holes,” *Phys. Rev. D* **109**, 064087 (2024), [arXiv:2311.13557 \[gr-qc\]](#).
 - [15] C. R. Ordóñez, A. Chakraborty, H. E. Camblong, M. O. Scully, and W. G. Unruh, “Quantum aspects of spacetime: A quantum optics view of acceleration radiation and black holes,” (2025), [arXiv:2508.17401 \[gr-qc\]](#).
 - [16] C. R. Ordóñez, A. Chakraborty, H. E. Camblong, M. O. Scully, and W. G. Unruh, “Quantum aspects of spacetime: A quantum optics view of acceleration radiation and black holes,” (2025), [arXiv:2508.17401 \[gr-qc\]](#).
 - [17] A. Azizi, H. E. Camblong, A. Chakraborty, C. R. Ordóñez, and M. O. Scully, “Quantum optics meets black hole thermodynamics via conformal quantum mechanics: II. Thermodynamics of acceleration radiation,” *Phys. Rev. D* **104** (2021), [10.1103/PhysRevD.104.084085](#), [arXiv:2108.07572 \[gr-qc\]](#).
 - [18] Nada Eissa, Carlos R. Ordóñez, and Gustavo Valdivia-Mera, “Horizon brightened acceleration radiation entropy in causal diamond geometry: A near-horizon perspective,” *Phys. Rev. D* **112**, 085030 (2025), [arXiv:2508.13493 \[hep-th\]](#).
 - [19] J. S. Ben-Benjamin *et al.*, “Unruh Acceleration Radiation Revisited,” *Int. J. Mod. Phys. A* **34**, 1941005 (2019), [arXiv:1906.01729 \[quant-ph\]](#).

- [20] S. A. Fulling and J. H. Wilson, “The Equivalence Principle at Work in Radiation from Unaccelerated Atoms and Mirrors,” *Phys. Scripta* **94**, 014004 (2019), [arXiv:1805.01013 \[quant-ph\]](#).
- [21] Erickson Tjoa, Robert B. Mann, and Eduardo Martin-Martinez, “Particle Detectors, Cavities, and the Weak Equivalence Principle,” *Phys. Rev. D* **98**, 085004 (2018), [arXiv:1807.07628 \[quant-ph\]](#).
- [22] Kushal Chakraborty and Bibhas Ranjan Majhi, “Detector response along null geodesics in black hole spacetimes and in a Friedmann-Lemaître-Robertson-Walker Universe,” *Phys. Rev. D* **100**, 045004 (2019), [arXiv:1905.10554 \[gr-qc\]](#).
- [23] Richard Lopp, Eduardo Martin-Martinez, and Don N. Page, “Relativity and quantum optics: accelerated atoms in optical cavities,” *Class. Quant. Grav.* **35**, 224001 (2018), [arXiv:1806.10158 \[quant-ph\]](#).
- [24] Richard Lopp, *Light-Matter Interaction Models in Relativistic Quantum Information*, Ph.D. thesis, U. Waterloo (main) (2021).
- [25] Anatoly A. Svidzinsky, Jonathan S. Ben-Benjamin, Stephen A. Fulling, and Don N. Page, “Excitation of an Atom by a Uniformly Accelerated Mirror through Virtual Transitions,” *Phys. Rev. Lett.* **121**, 071301 (2018).
- [26] Anatoly A. Svidzinsky, “Excitation of a uniformly moving atom through vacuum fluctuations,” *Phys. Rev. Res.* **1**, 033027 (2019).
- [27] E. Sadurní, M. A. Estévez, and J. L. Díaz-Cruz, “Does an accelerated mirror suffer hindrance from vacuum?” (2021), [arXiv:2109.09295 \[gr-qc\]](#).
- [28] Michael R. R. Good and Eric V. Linder, “Quantum power: a Lorentz invariant approach to Hawking radiation,” *Eur. Phys. J. C* **82**, 204 (2022), [arXiv:2111.15148 \[gr-qc\]](#).
- [29] Ashmita Das and Bibhas Ranjan Majhi, “Unruh-Fulling effect in nonlocal field theory: The role of Unruh decomposition,” *Phys. Rev. D* **106**, 105025 (2022), [arXiv:2204.13513 \[hep-th\]](#).
- [30] Georgy Y. Prokhorov, Oleg V. Teryaev, and Valentin I. Zakharov, “Calculation of acceleration effects using the Zubarev density operator,” *Particles* **3**, 1–14 (2020), [arXiv:1911.04563 \[hep-th\]](#).
- [31] Ashmita Das, Soham Sen, and Sunandan Gangopadhyay, “Virtual transitions in an atom-mirror system in the presence of two scalar photons,” *Phys. Rev. D* **107**, 025009 (2023), [arXiv:2208.12021 \[quant-ph\]](#).
- [32] Francesco Sorge and Justin H. Wilson, “Casimir effect and free fall in a Schwarzschild black hole,” in *15th Marcel Grossmann Meeting on Recent Developments in Theoretical and Experimental General Relativity, Astrophysics, and Relativistic Field Theories* (2018) [arXiv:1807.03968 \[gr-qc\]](#).
- [33] Helder A. S. Costa, Irismar G. da Paz, Paulo R. S. Carvalho, and Marcos Sampaio, “Ramsey interferometry as a witness of acceleration radiation,” *Annals Phys.* **416**, 168158 (2020), [arXiv:2008.03112 \[quant-ph\]](#).
- [34] Syed Masood, “A Casimir-like probe for 4D Einstein-Gauss-Bonnet gravity,” (2024), [arXiv:2407.02313 \[gr-qc\]](#).
- [35] Chenni Xu and Li-Gang Wang, “Theory of light propagation in arbitrary two-dimensional curved space,” (2021), [arXiv:2109.14702 \[physics.optics\]](#).
- [36] Yongjie Pan and Baocheng Zhang, “Gravity-induced transparency,” *Phys. Rev. D* **109**, 125018 (2024), [arXiv:2406.01227 \[hep-th\]](#).
- [37] Georgi Gary Rozenman, Freyja Ullinger, Matthias Zimmermann, Maxim A. Efremov, Lev Shemer, Wolfgang P. Schleich, and Ady Arie, “Observation of a phase space horizon with surface gravity water waves,” *Commun. Phys.* **7**, 165 (2024).
- [38] Francesco Sorge, “Jaynes–Cummings model in a weak gravitational wave background,” *Class. Quant. Grav.* **41**, 015028 (2024).
- [39] Tyler Christian McMaken, *Quantum Effects Inside Rotating, Accreting Black Holes*, Ph.D. thesis, Colorado U., Colorado U. (2024).
- [40] Syed Masood A. S. Bukhari and Li-Gang Wang, “Atom-field dynamics in curved spacetime,” *Front. Phys. (Beijing)* **19**, 54203 (2024), [arXiv:2307.12222 \[gr-qc\]](#).
- [41] Fujin Wang, Syed Masood, and L. G. Wang, “Quantum light and radiation in Rindler spacetime: from uncertainty relations to the cosmological implications,” (2025), [arXiv:2506.02417 \[gr-qc\]](#).
- [42] Magdalena Zych, Łukasz Rudnicki, and Igor Pikovski, “Gravitational mass of composite systems,” *Phys. Rev. D* **99**, 104029 (2019), [arXiv:1808.05831 \[gr-qc\]](#).
- [43] Riddhi Chatterjee, Sunandan Gangopadhyay, and A. S. Majumdar, “Violation of equivalence in an accelerating atom-mirror system in the generalized uncertainty principle framework,” *Phys. Rev. D* **104**, 124001 (2021), [arXiv:2104.10531 \[quant-ph\]](#).
- [44] Riddhi Chatterjee, Sunandan Gangopadhyay, and A. S. Majumdar, “Resonance interaction of two entangled atoms accelerating between two mirrors,” *Eur. Phys. J. D* **75**, 179 (2021), [arXiv:2007.15465 \[quant-ph\]](#).
- [45] Subhajit Barman and Bibhas Ranjan Majhi, “Radiative process of two entangled uniformly accelerated atoms in a thermal bath: a possible case of anti-Unruh event,” *JHEP* **03**, 245 (2021), [arXiv:2101.08186 \[gr-qc\]](#).
- [46] Shujuan Liu and Hongwei Xiong, “On the Thermodynamic Origin of Gravitational Force by Applying Spacetime Entanglement Entropy and the Unruh Effect,” *Entropy* **21**, 296 (2019).
- [47] Surojit Dalui and Bibhas Ranjan Majhi, “Near horizon local instability and quantum thermality,” *Phys. Rev. D* **102**, 124047 (2020), [arXiv:2007.14312 \[gr-qc\]](#).
- [48] Soham Sen, Rituparna Mandal, and Sunandan Gangopadhyay, “Near horizon aspects of acceleration radiation of an atom falling into a class of static spherically symmetric black hole geometries,” *Phys. Rev. D* **106**, 025004 (2022), [arXiv:2205.11260 \[gr-qc\]](#).
- [49] Surojit Dalui, *Classical and Quantum Aspects of Near-Horizon Physics*, Ph.D. thesis, Indian Inst. Tech., Guwahati (2023).
- [50] Kensuke Gallock-Yoshimura, Erickson Tjoa, and Robert B. Mann, “Harvesting entanglement with detectors freely falling into a black hole,” *Phys. Rev. D* **104**, 025001 (2021), [arXiv:2102.09573 \[quant-ph\]](#).
- [51] Subhajit Barman, Dipankar Barman, and Bibhas Ranjan Majhi, “Entanglement harvesting from conformal vacuums

- between two Unruh-DeWitt detectors moving along null paths,” *JHEP* **09**, 106 (2022), [arXiv:2112.01308 \[gr-qc\]](#).
- [52] Subhajit Barman and Bibhas Ranjan Majhi, “Optimization of entanglement depends on whether a black hole is extremal,” *Gen. Rel. Grav.* **56**, 70 (2024), [arXiv:2301.06764 \[gr-qc\]](#).
- [53] D. Jaffino Stargen and Vivishek Sudhir, “Thermality and athermalty in the Unruh effect,” (2025), [arXiv:2509.01983 \[gr-qc\]](#).
- [54] Yusef Maleki, Bahram Ahansaz, Kangle Li, and Alireza Maleki, “Quantum Steering Ellipsoid and Unruh Effect,” (2021), [arXiv:2110.14866 \[quant-ph\]](#).
- [55] Yining You and Sheng-Wen Li, “Entropy dynamics of a dephasing model in a squeezed thermal bath,” *Phys. Rev. A* **97**, 012114 (2018), [arXiv:1709.05764 \[quant-ph\]](#).
- [56] Zehua Tian, Jiliang Jing, and Jiangfeng Du, “Direct characteristic-function tomography of the quantum states of quantum fields,” *Sci. China Phys. Mech. Astron.* **66**, 110412 (2023), [arXiv:2310.13530 \[quant-ph\]](#).
- [57] Riddhi Chatterjee and A. S. Majumdar, “Bell-inequality violation by dynamical Casimir photons in a superconducting microwave circuit,” *Phys. Rev. A* **106**, 042224 (2022), [arXiv:2202.05824 \[quant-ph\]](#).
- [58] H. T. Lopes, I. G. da Paz, P. R. S. Carvalho, and H. A. S. Costa, “Thermal signature of the Unruh effect in the interference pattern,” *Phys. Lett. A* **409**, 127483 (2021).
- [59] Bibhas Ranjan Majhi, “Shock wave quantum memory in shocked detector,” *Mod. Phys. Lett. A* **36**, 2150186 (2021), [arXiv:2108.01307 \[gr-qc\]](#).
- [60] Avijit Misra, Pritam Chattopadhyay, Anatoly Svidzinsky, Marlan O. Scully, and Gershon Kurizki, “Black-hole powered quantum coherent amplifier,” *npj Quantum Inf.* **10**, 34 (2024), [arXiv:2307.04672 \[quant-ph\]](#).
- [61] Roland E. Allen, “Black hole entropy, the black hole information paradox, and time travel paradoxes from a new perspective,” *J. Mod. Opt.* **67**, 35–40 (2020), [arXiv:1901.09096 \[physics.gen-ph\]](#).
- [62] Stefano Longhi, “Laser Mpemba effect,” *Opt. Lett.* **50**, 2069–2072 (2025), [arXiv:2503.14989 \[quant-ph\]](#).
- [63] J. S. Ben-Benjamin *et al.*, “Unruh Acceleration Radiation Revisited,” *Int. J. Mod. Phys. A* **34**, 1941005 (2019), [arXiv:1906.01729 \[quant-ph\]](#).
- [64] Soham Sen, Rituparna Mandal, and Sunandan Gangopadhyay, “Equivalence principle and HBAR entropy of an atom falling into a quantum corrected black hole,” *Phys. Rev. D* **105**, 085007 (2022), [arXiv:2202.00671 \[hep-th\]](#).
- [65] Arpita Jana, Soham Sen, and Sunandan Gangopadhyay, “Atom falling into a quantum corrected charged black hole and HBAR entropy,” *Phys. Rev. D* **110**, 026029 (2024), [arXiv:2405.13087 \[gr-qc\]](#).
- [66] Arpita Jana, Soham Sen, and Sunandan Gangopadhyay, “Inverse logarithmic correction in the horizon brightened acceleration radiation entropy of an atom falling into a renormalization group improved charged black hole,” *Phys. Rev. D* **111**, 085017 (2025), [arXiv:2501.17579 \[gr-qc\]](#).
- [67] Soham Sen, Rituparna Mandal, and Sunandan Gangopadhyay, “Near horizon approximation and beyond for a two-level atom falling into a Kerr–Newman black hole,” *Eur. Phys. J. Plus* **138**, 855 (2023), [arXiv:2301.04834 \[gr-qc\]](#).
- [68] Syed Masood A. S. Bukhari, Imtiaz Ahmad Bhat, Chennai Xu, and Li-Gang Wang, “Nonthermal acceleration radiation of atoms near a black hole in presence of dark energy,” *Phys. Rev. D* **107**, 105017 (2023), [arXiv:2211.08793 \[gr-qc\]](#).
- [69] Syed Masood A. S. Bukhari and Li-Gang Wang, “Seeing dark matter via acceleration radiation,” *Phys. Rev. D* **109**, 045009 (2024), [arXiv:2309.11958 \[gr-qc\]](#).
- [70] Ashmita Das, Anjana Krishnan, Soham Sen, and Sunandan Gangopadhyay, “Derivative coupling in horizon brightened acceleration radiation: A quantum optics approach,” *Phys. Rev. D* **112**, 065006 (2025), [arXiv:2505.16897 \[gr-qc\]](#).
- [71] Reggie C. Pantig and Ali Övgün, “Acceleration radiation from derivative-coupled atoms falling in modified gravity black holes,” *Eur. Phys. J. C* **85**, 1183 (2025), [arXiv:2508.11734 \[gr-qc\]](#).
- [72] Ali Övgün and Reggie C. Pantig, “HBAR entropy of Infalling Atoms into a GUP-corrected Schwarzschild Black Hole and equivalence principle,” (2025), [arXiv:2506.10621 \[gr-qc\]](#).
- [73] Yu Tang, Wentao Liu, and Jieci Wang, “Observational signature of Lorentz violation in acceleration radiation,” *Eur. Phys. J. C* **85**, 1108 (2025), [arXiv:2502.03043 \[gr-qc\]](#).
- [74] Anisur Rahaman, “Radiative transition of an atom falling into spherically symmetric Lorentz violating black hole background,” (2025), [arXiv:2503.23553 \[gr-qc\]](#).
- [75] Anisur Rahaman, “An atom in front of Lorentz violating Kalb-Ramond black hole background,” (2025), [arXiv:2506.01006 \[hep-th\]](#).
- [76] Freyja Ullinger, Matthias Zimmermann, and Wolfgang P. Schleich, “The logarithmic phase singularity in the inverted harmonic oscillator,” *AVS Quantum Sci.* **4**, 024402 (2022).
- [77] Nitesh K. Dubey and Sanved Kolekar, “Wigner distributions in Rindler spacetime and nonvacuum Minkowski states,” *Phys. Rev. D* **111**, 065004 (2025), [arXiv:2409.10054 \[gr-qc\]](#).
- [78] Gianluca Gregori, Giacomo Marocco, Subir Sarkar, Robert Bingham, and Charles Wang, “Measuring Unruh radiation from accelerated electrons,” *Eur. Phys. J. C* **84**, 475 (2024), [arXiv:2301.06772 \[gr-qc\]](#).
- [79] D. Maksimović, M. Nieslony, and M. Wurm, “ConvNets for Enhanced Background Discrimination in the Diffuse Supernova Neutrino Background Search,” *Astrophys. Space Sci. Proc.* **60**, 173–178 (2023).
- [80] Emanuele Berti, Vitor Cardoso, and Andrei O. Starinets, “Quasinormal modes of black holes and black branes,” *Class. Quant. Grav.* **26**, 163001 (2009), [arXiv:0905.2975 \[gr-qc\]](#).
- [81] R. A. Konoplya and A. Zhidenko, “Quasinormal modes of black holes: From astrophysics to string theory,” *Rev. Mod. Phys.* **83**, 793–836 (2011), [arXiv:1102.4014 \[gr-qc\]](#).
- [82] Kostas D. Kokkotas and Bernd G. Schmidt, “Quasinormal modes of stars and black holes,” *Living Rev. Rel.* **2**, 2 (1999), [arXiv:gr-qc/9909058](#).

- [83] Hans-Peter Nollert, “TOPICAL REVIEW: Quasinormal modes: the characteristic ‘sound’ of black holes and neutron stars,” *Class. Quant. Grav.* **16**, R159–R216 (1999).
- [84] Clarissa-Marie Claudel, K. S. Virbhadra, and G. F. R. Ellis, “The Geometry of photon surfaces,” *J. Math. Phys.* **42**, 818–838 (2001), [arXiv:gr-qc/0005050](#).
- [85] K. S. Virbhadra and G. F. R. Ellis, “Gravitational lensing by naked singularities,” *Phys. Rev. D* **65**, 103004 (2002).
- [86] Stephen L. Adler and K. S. Virbhadra, “Cosmological constant corrections to the photon sphere and black hole shadow radii,” *Gen. Rel. Grav.* **54**, 93 (2022), [arXiv:2205.04628 \[gr-qc\]](#).
- [87] Sunny Vagnozzi *et al.*, “Horizon-scale tests of gravity theories and fundamental physics from the Event Horizon Telescope image of Sagittarius A,” *Class. Quant. Grav.* **40**, 165007 (2023), [arXiv:2205.07787 \[gr-qc\]](#).
- [88] Alireza Allahyari, Mohsen Khodadi, Sunny Vagnozzi, and David F. Mota, “Magnetically charged black holes from non-linear electrodynamics and the Event Horizon Telescope,” *JCAP* **02**, 003 (2020), [arXiv:1912.08231 \[gr-qc\]](#).
- [89] Mohsen Khodadi, Alireza Allahyari, Sunny Vagnozzi, and David F. Mota, “Black holes with scalar hair in light of the Event Horizon Telescope,” *JCAP* **09**, 026 (2020), [arXiv:2005.05992 \[gr-qc\]](#).
- [90] Farruh Atamurotov, Ahmadjon Abdujabbarov, and Bobomurat Ahmedov, “Shadow of rotating non-Kerr black hole,” *Phys. Rev. D* **88**, 064004 (2013).
- [91] Farruh Atamurotov and Bobomurat Ahmedov, “Optical properties of black hole in the presence of plasma: shadow,” *Phys. Rev. D* **92**, 084005 (2015), [arXiv:1507.08131 \[gr-qc\]](#).
- [92] Ahmadjon Abdujabbarov, Farruh Atamurotov, Naresh Dadhich, Bobomurat Ahmedov, and Zdeněk Stuchlík, “Energetics and optical properties of 6-dimensional rotating black hole in pure Gauss–Bonnet gravity,” *Eur. Phys. J. C* **75**, 399 (2015), [arXiv:1508.00331 \[gr-qc\]](#).
- [93] Ahmadjon Abdujabbarov, Bobomurat Ahmedov, Naresh Dadhich, and Farruh Atamurotov, “Optical properties of a braneworld black hole: Gravitational lensing and retrolensing,” *Phys. Rev. D* **96**, 084017 (2017).
- [94] Edward W. Leaver, “Spectral decomposition of the perturbation response of the Schwarzschild geometry,” *Phys. Rev. D* **34**, 384–408 (1986).
- [95] Nils Andersson, “Evolving test fields in a black hole geometry,” *Phys. Rev. D* **55**, 468–479 (1997), [arXiv:gr-qc/9607064](#).
- [96] Marc Casals, Sam Dolan, Adrian C. Ottewill, and Barry Wardell, “Self-Force and Green Function in Schwarzschild spacetime via Quasinormal Modes and Branch Cut,” *Phys. Rev. D* **88**, 044022 (2013), [arXiv:1306.0884 \[gr-qc\]](#).
- [97] Vitor Cardoso and Jose P. S. Lemos, “Quasinormal modes of Schwarzschild anti-de Sitter black holes: Electromagnetic and gravitational perturbations,” *Phys. Rev. D* **64**, 084017 (2001), [arXiv:gr-qc/0105103](#).
- [98] A. Zhidenko, “Quasinormal modes of Schwarzschild de Sitter black holes,” *Class. Quant. Grav.* **21**, 273–280 (2004), [arXiv:gr-qc/0307012](#).
- [99] Rodrigo Aros, Cristian Martinez, Ricardo Troncoso, and Jorge Zanelli, “Quasinormal modes for massless topological black holes,” *Phys. Rev. D* **67**, 044014 (2003), [arXiv:hep-th/0211024](#).
- [100] Sharmanthie Fernando and Juan Correa, “Quasinormal Modes of Bardeen Black Hole: Scalar Perturbations,” *Phys. Rev. D* **86**, 064039 (2012), [arXiv:1208.5442 \[gr-qc\]](#).
- [101] Bobir Toshmatov, Ahmadjon Abdujabbarov, Zdeněk Stuchlík, and Bobomurat Ahmedov, “Quasinormal modes of test fields around regular black holes,” *Phys. Rev. D* **91**, 083008 (2015), [arXiv:1503.05737 \[gr-qc\]](#).
- [102] Ángel Rincón and Grigoris Panotopoulos, “Quasinormal modes of scale dependent black holes in $(1+2)$ -dimensional Einstein-power-Maxwell theory,” *Phys. Rev. D* **97**, 024027 (2018), [arXiv:1801.03248 \[hep-th\]](#).
- [103] R. A. Konoplya and A. F. Zinhailo, “Quasinormal modes, stability and shadows of a black hole in the 4D Einstein–Gauss–Bonnet gravity,” *Eur. Phys. J. C* **80**, 1049 (2020), [arXiv:2003.01188 \[gr-qc\]](#).
- [104] Reggie C. Pantig, Leonardo Mastrototaro, Gaetano Lambiase, and Ali Övgün, “Shadow, lensing, quasinormal modes, greybody bounds and neutrino propagation by dyonic ModMax black holes,” *Eur. Phys. J. C* **82**, 1155 (2022), [arXiv:2208.06664 \[gr-qc\]](#).
- [105] Guoyang Fu, Dan Zhang, Peng Liu, Xiao-Mei Kuang, Qiyuan Pan, and Jian-Pin Wu, “Quasinormal modes and Hawking radiation of a charged Weyl black hole,” *Phys. Rev. D* **107**, 044049 (2023), [arXiv:2207.12927 \[gr-qc\]](#).
- [106] Guoyang Fu, Dan Zhang, Peng Liu, Xiao-Mei Kuang, and Jian-Pin Wu, “Peculiar properties in quasinormal spectra from loop quantum gravity effect,” *Phys. Rev. D* **109**, 026010 (2024), [arXiv:2301.08421 \[gr-qc\]](#).
- [107] Sam R. Dolan, “Instability of the massive Klein-Gordon field on the Kerr spacetime,” *Phys. Rev. D* **76**, 084001 (2007), [arXiv:0705.2880 \[gr-qc\]](#).
- [108] Sam R. Dolan, “The Quasinormal Mode Spectrum of a Kerr Black Hole in the Eikonal Limit,” *Phys. Rev. D* **82**, 104003 (2010), [arXiv:1007.5097 \[gr-qc\]](#).
- [109] Paolo Pani, Vitor Cardoso, Leonardo Gualtieri, Emanuele Berti, and Akihiro Ishibashi, “Perturbations of slowly rotating black holes: massive vector fields in the Kerr metric,” *Phys. Rev. D* **86**, 104017 (2012), [arXiv:1209.0773 \[gr-qc\]](#).
- [110] Valeri P. Frolov, Pavel Krtoš, David Kubizňák, and Jorge E. Santos, “Massive Vector Fields in Rotating Black-Hole Spacetimes: Separability and Quasinormal Modes,” *Phys. Rev. Lett.* **120**, 231103 (2018), [arXiv:1804.00030 \[hep-th\]](#).
- [111] R. A. Konoplya and Z. Stuchlík, “Are eikonal quasinormal modes linked to the unstable circular null geodesics?” *Phys. Lett. B* **771**, 597–602 (2017), [arXiv:1705.05928 \[gr-qc\]](#).
- [112] R. A. Konoplya, A. Zhidenko, and A. F. Zinhailo, “Higher order WKB formula for quasinormal modes and grey-body factors: recipes for quick and accurate calculations,” *Class. Quant. Grav.* **36**, 155002 (2019), [arXiv:1904.10333 \[gr-qc\]](#).
- [113] Ramin G. Daghighi, Michael D. Green, and Jodin C. Morey, “Calculating quasinormal modes of Schwarzschild anti-de Sitter black holes using the continued fraction method,” *Phys. Rev. D* **107**, 024023 (2023), [arXiv:2209.09324 \[gr-qc\]](#).
- [114] Wei-Liang Qian, Kai Lin, Xiao-Mei Kuang, Bin Wang, and Rui-Hong Yue, “Quasinormal modes in two-photon autocor-

- relation and the geometric-optics approximation,” *Eur. Phys. J. C* **82**, 188 (2022), [arXiv:2109.02844 \[gr-qc\]](#).
- [115] Ramin G. Daghighi, Michael D. Green, and Jodin C. Morey, “Significance of Black Hole Quasinormal Modes: A Closer Look,” *Phys. Rev. D* **101**, 104009 (2020), [arXiv:2002.07251 \[gr-qc\]](#).
 - [116] Ramin G. Daghighi, Michael D. Green, and Gabor Kunstatter, “Scalar Perturbations and Stability of a Loop Quantum Corrected Kruskal Black Hole,” *Phys. Rev. D* **103**, 084031 (2021), [arXiv:2012.13359 \[gr-qc\]](#).
 - [117] Ramin G. Daghighi, Michael D. Green, Jodin C. Morey, and Gabor Kunstatter, “Scalar Perturbations of a Single-Horizon Regular Black Hole,” *Phys. Rev. D* **102**, 104040 (2020), [arXiv:2009.02367 \[gr-qc\]](#).
 - [118] Oscar J. C. Dias, Mahdi Godazgar, and Jorge E. Santos, “Linear Mode Stability of the Kerr-Newman Black Hole and Its Quasinormal Modes,” *Phys. Rev. Lett.* **114**, 151101 (2015), [arXiv:1501.04625 \[gr-qc\]](#).
 - [119] Shui-Fa Shen, Guan-Ru Li, Ramin G. Daghighi, Jodin C. Morey, Michael D. Green, Wei-Liang Qian, and Rui-Hong Yue, “Asymptotic quasinormal modes, echoes, and black hole spectral instability: a brief review,” (2025), [arXiv:2507.11663 \[gr-qc\]](#).
 - [120] M. O. Scully and M. S. Zubairy, *Quantum Optics* (Cambridge University Press, Cambridge, UK, 1997).
 - [121] Vitor Cardoso, Alex S. Miranda, Emanuele Berti, Helvi Witek, and Vilson T. Zanchin, “Geodesic stability, Lyapunov exponents and quasinormal modes,” *Phys. Rev. D* **79**, 064016 (2009), [arXiv:0812.1806 \[hep-th\]](#).
 - [122] Tullio Regge and John A. Wheeler, “Stability of a Schwarzschild singularity,” *Phys. Rev.* **108**, 1063–1069 (1957).
 - [123] Frank J. Zerilli, “Effective potential for even parity Regge-Wheeler gravitational perturbation equations,” *Phys. Rev. Lett.* **24**, 737–738 (1970).
 - [124] N. Andersson, “Excitation of Schwarzschild black hole quasinormal modes,” *Phys. Rev. D* **51**, 353–363 (1995).